 doi:10.20944/preprints202007.0138.v1

RESEARCH ARTICLE

Cavitation in Pharmaceutical Manufacturing

Donn Sederstrom[1], Rafael Valotta Rodrigues [2]* and Corinne Lengsfeld [3],

Received: 24 June 2020; Accepted: date; Published: date.

Therapeutic proteins are used to successfully treat hemophilia, Crohn's Disease, diabetes, and cancer. Recent product recalls have occurred because of sub-visible particle formation resulting from the inherent instability of proteins. It has been suggested that particle formation is associated with late stage processing steps of filling, shipping, and delivery. Previous works demonstrated that cavitation might occur in therapeutic vials subjected to agitation or accidentally dropped, but that mitigation can be achieved with fluid property manipulation. The goal of this research was to (1) assess the risk of cavitation under common pharmaceutical manufacturing conditions (i.e., pipe contraction and pumps), (2) establish a simple threshold criterion for when particulate will form, and (3) suggest a series of mitigation techniques based on these thresholds. To accomplish these tasks, computational fluid dynamic simulations for a variety of pipe contraction and fluid properties were performed. The results of this research show that reducing the turbulence in a fluid system will reduce the likelihood of cavitation. Additionally, threshold bounds were created that establish a definitive transition at which cavitation will occur.

Therapeutic proteins are used to treat hemophilia, Crohn's Disease, diabetes, and cancer[1]. These proteins are inherently unstable which can cause them to denature and aggregate[1-5]. If the patient is to receive the therapeutic protein's designed effect, the protein must be delivered in its native state. Studies have shown that there can be adverse effects if proteins are not in their native state. These adverse effects can include reduction in responsiveness to the drug therapy, eventually leading to immunogenicity[3-10]. Studies have also shown that therapeutic proteins are highly susceptible to degradation because of their weak bonding structures[2]. The use of therapeutic proteins is on the rise as they are becoming more affordable, and the availability of drugs has increased in recent years[2]. Additionally, pharmaceutical companies are increasing the scale of production resulting in filling vials and syringes in a rapid manner. The use of larger equipment due to the increase in the production rate can lead to increased fluid flow rates, pressures, and vibrations, all of which lead to protein instability[11]. The focus of this research will be on physical instabilities causing protein degradation, specifically investigating the role of cavitation.

Mass Production of Therapeutic Proteins

In order to bring a therapeutic protein to the market, companies spend years and extensive resources to create and cultivate exact strands of proteins[12]. When making these new proteins, companies begin with small scale equipment to grow and cultivate the new proteins leading to animal testing, human testing, and eventually Food and Drug Administration (FDA) approval for

[1] **Johns Manville Company, Denver, Colorado**
[2] **Syracuse University, Mechanical and Aerospace Engineering Department**
[3] **University of Denver, Mechanical and Materials Engineering Department**
Corresponding author: (+1) 720 810 8349 rvrodrig@syr.edy

Preprints (www.preprints.org) | NOT PEER-REVIEWED | Posted: 7 July 2020 doi:10.20944/preprints202007.0138.v1

human use. In this process, the company is not worried about the quantity of therapeutic protein produced, the priority is the quality of the end product used to gain FDA approval. Once a drug is approved for use in humans and available on the market, companies increase production with the goal of producing more drugs more efficiently. To do this, the pharmaceutical solution is pumped at higher speeds and pressures to increase the efficiency of the manufacturing process. Additionally, the piping, pumping, and associated valves used to transport the solution are altered because of the new specifications for larger sizes, higher flow rates, and higher pressures. The significance of the changes in fluid and flow properties when machinery is changed from small to large scale is not evaluated, therefore the retrofitted system has a high potential to cavitate.

Cavitation

Cavitation is a phenomenon where a liquid flash boils to vapor and then collapses. Although there are some proposed methods to harness hydrodynamic cavitation in ways to increase pharmaceutic manufacturing efficiency[13,14], cavitation is usually an undesirable phenomenon. The flash boiling that occurs with cavitation can be caused by hydrodynamic, mechanical, or acoustic forces that lower the local pressure to below the critical pressure. Because this is a local phenomenon, once the external force driving the low pressure is removed, pressure returns rapidly to the bulk value and the vapor bubble rapidly collapses. During the collapse of the vapor bubble to the bulk fluid, high velocities are present and collide at a singularity point creating high pressures and large amounts of localized heat. The subsequent dissociation of water can occur, which generates free radicals. These are localized phenomena making the temperature and pressure gradient extremely high at the site of cavitation[15]. Although the primary key to understanding when cavitation occurs is well defined, the factors that reduce its onset and likelihood are not widely documented.

Traditionally, it is understood that a fluid will cavitate when the vapor pressure of the fluid is equal or greater than the local low pressure. This is true when no turbulence is present. However, when turbulence is present a fluid will cavitate at a higher pressure called the critical pressure. The vapor pressure is computed by the Clausius Clapeyron equation which is a function of the temperature of the fluid, Equation 1[16]. Several methods have been proposed to calculate the critical pressure[17]. For this application and under these conditions, the most appropriate equation for the critical pressure is derived by Singhal et al.[18], Equation 2, because it utilized the turbulent kinetic energy to account for turbulence in the model. This results in a critical pressure equal to the vapor pressure when turbulence is not present and an increase in the critical pressure when turbulence is present.

$$log_{10}(P_{vap}) = A - \frac{B}{T + C - 273.15} \tag{1}$$

$$P_c = P_{vap} + 0.195\rho k \tag{2}$$

Preprints (www.preprints.org) | NOT PEER-REVIEWED | Posted: 7 July 2020 doi:10.20944/preprints202007.0138.v1

Where P_{vap} is the vapor pressure of the fluid, T is the temperature of the fluid, and A, B, and C are experimentally determined constants provided by Poling et al.[16], P_c is the critical pressure, ρ is density, and k is the turbulent kinetic energy (check literature[19] for more information about k).

Modeling Cavitation

Due to the complexity of cavitation and the different ways this phenomenon can occur, modeling cavitation is challenging. Not only does modeling cavitation require a detailed understanding of when a flow cavitates to form a vapor bubble, it also requires understanding when a vapor bubble will collapse back into the bulk fluid. For specific applications, codes can be created and applied on an individual basis, but a generic code that applies across all applications of cavitation is much more challenging. The available codes for specific application include cavitation due to hydrofoils, shock waves, turbulence, and high speed propellers[20-27]. These models are only valid for their specific application. Singhal et. al. has produced several specific models that are appropriate for this application. Singhal's "Full Cavitation Model" utilizes a robust algorithm with generic cavitation application and allows the cavitation point to be specified directly by the user[18]. The Full Cavitation Model is currently being utilized by industry and commercially available Computational Fluid Dynamics (CFD) software to model water and oil pumps, inducers, impellers, and fuel injection systems[18].

Proteins Denaturation

The ionic and covalent bonds holding the molecules in the protein together are very strong, but, in comparison, the secondary bonds holding the shape and structure of the protein are relatively weaker. These secondary bonds can be broken by either chemical or physical instabilities[2]. Physical instabilities include denaturation, aggregation, precipitation, and absorption[2]. When these unique bond structures and shapes of therapeutic protein are broken, the proteins become partially or fully unfolded. These unfolded proteins can group together to form large aggregates. These larger aggregates are regulated by the FDA and are blamed for the adverse effects seen in patients[3-10]. Recent studies have shown that smaller aggregates, in comparison to previous research, still have the potential to cause adverse effect in patients even though they are not regulated by the FDA[28].

Several factors can lead to protein unfolding and aggregation such as amino acid sequence, pH level, temperature, and concentration[28]. Additionally, these proteins have highly hydrophobic and hydrophilic parts. Because of this, when the protein comes in contact with a gas-liquid interface, it is pushed and pulled to the point where they can change shape and unfold. In terms of protein stability, cavitation results in at least two events that are undesired. The large temperature gradients and additional gas-liquid interfaces produced by cavitation are undesirable because of their potential to cause protein degradation.

The research involving protein stability was first documented by Hsien We in 1931, but the application of proteins to patients for therapeutic effects is still considered a new treatment[29]. Previous research using an ultrasonic nebulizer to vaporize protein has demonstrated that cavitation causes protein degradation and the proteins are the sites for nucleation[5]. Additional

Preprints (www.preprints.org) | NOT PEER-REVIEWED | Posted: 7 July 2020 doi:10.20944/preprints202007.0138.v1

research has shown therapeutic protein degradation occurs in the process of shipping proteins to the patient or distributer[28,30].

Dimensionless Numbers

Classically, the relative importance of geometry, fluid properties, and flow conditions on hydrodynamic phenomena is not conducted via dimensional quantities. Instead non-dimensional terms are utilized to enable the transfer of the information to a broad range of applications as desired in this case.

Diameter ratio can be used to characterize the geometric configuration of a contracting or expanding flow. It is defined as a ratio of minor diameter to major diameter, Equation 3, where D_r is the diameter ratio, D_{minor} is the minor diameter at the outlet, and D_{major} is the major diameter at the inlet.

$$D_r = \frac{D_{minor}}{D_{major}} \tag{3}$$

The Reynolds number (R_e)is the most readily used non-dimensional number in fluid dynamics. It provides the relative ratio of inertial to viscous effects. Although frequently used to monitor the transition from laminar to turbulent flow, it also provides a tool for non-dimensionally describing the dynamic or velocity effects. In Equation 4, ρ is the density of the solutions, ν is the mean velocity of the fluid, D is the characteristic length, and μ is the dynamic viscosity of the fluid.

$$Re = \frac{\rho v \mathrm{D}}{\mu} \tag{4}$$

Cavitation number is a dimensionless number used to characterize the likelihood of a fluid to cavitate via a ratio of pressure difference between the local flow pressure and vapor pressure of the fluid in relation to the dynamic pressure of the system. The Cavitation number is independent of both the flow geometry and turbulence energy in the flow, see Equation 5, where C_a is the Cavitation number and P_{local} is the absolute pressure at a point in the fluid. The cavitation number evaluated in this work was the global minimum cavitation number, and P_{local} was determined by taking the minimum pressure over value over the entire model. In the geometry modeled, the local minimum occurred near the edge of the flow constriction.

$$Ca = \frac{P_{local} - P_{vap}}{\frac{1}{2}\rho v^2} \tag{5}$$

The pressure drop along the flow direction of a pipe is magnified by the addition of a constriction. The pressure recovery coefficient, C_p, quantifies this pressure loss normalized by the dynamic pressure, Equation 6. P_{out} is the pressure at the outlet and P_{in} is the pressure of the inlet.

$$C_p = \frac{P_{out} - P_{in}}{\frac{1}{2}\rho v^2} \tag{6}$$

Preprints (www.preprints.org) | NOT PEER-REVIEWED | Posted: 7 July 2020 doi:10.20944/preprints202007.0138.v1

None of the previous non-dimensional quantities explored the significance of the maximum principal stress or turbulence on the potential for a flow to cavitate. As this can lower the critical pressure by 2-fold, its importance should likely not be ignored. Thus, it is important to quantify the Kolmogorov length scale and the energy dissipation rate by developing associated dimensionless parameters.

The Kolmogorov length scale is a length that characterizes the smallest eddies in a flow [31]. Energy is dissipated in a fluid flow through the energy cascade of eddy dissipation. In each eddy, there are two smaller eddies that transfer the energy to a smaller and smaller length scale. The cascade continues until the Kolmogorov length scale is reached which is indicated by no more smaller eddies and at which point the energy is transferred into heat which is dissipated by the fluid. This energy dissipation happens at all scales of fluid flow. The Kolmogorov length scale is determined by the viscous forces over energy dissipation per mass, Equation 7, where η is the Kolmogorov length scale, γ is the kinematic viscosity, and ε is the energy dissipation rate.

$$\eta = \left(\frac{\gamma^3}{\varepsilon}\right)^{1/4} \tag{7}$$

The energy dissipation of the fluid was determined by the energy introduced in the system per unit mass. This was calculated using Equation 8 derived from Lengsfeld et al.[32] where $\dot{m}$ is the mass flow rate, and m is the mass in the system.

$$\varepsilon = \frac{(P_{in} - P_{out})\dot{m}}{m} \tag{8}$$

Methods

Model Description: To provide a controlled model that represents a range of pharmaceutical manufacturing processes, with the potential to cavitate, a constricting square-edge channel was created, as in Figure 1. Parameters that should impact the probability of cavitation in a flow are the fluid properties, the flow properties, and the geometric properties, which will be altered to span conditions found in syringe injection and rapid vial filling. A pipe constriction is a good representation of a commonly occurring feature where cavitation is likely to occur, and this feature is present in piping systems, pumps, and syringes. The fluid, flow, and geometric parameters altered were: major diameter (i.e., inlet), Minor diameter (i.e., outlet), Mass flow rate, Viscosity, Constriction edge type, and Density.

Preprints (www.preprints.org) | NOT PEER-REVIEWED | Posted: 7 July 2020 doi:10.20944/preprints202007.0138.v1

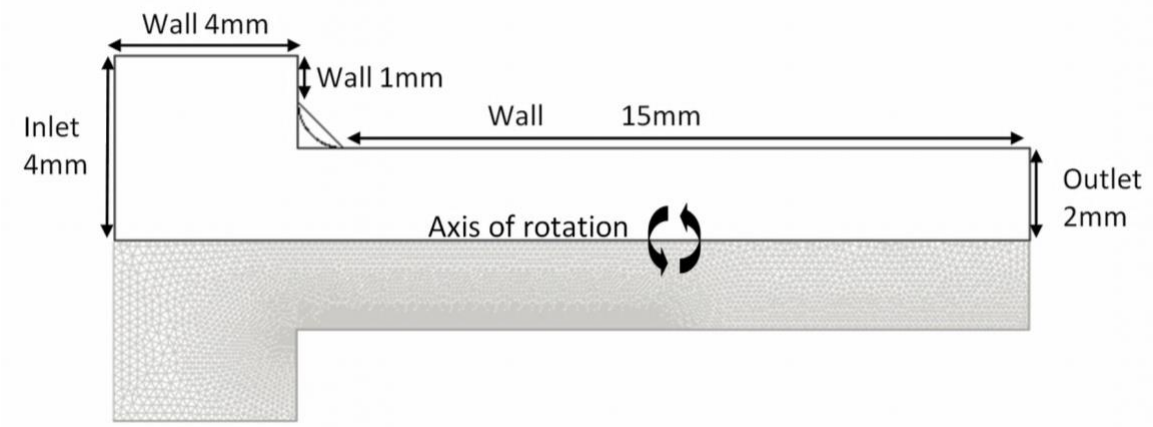

Figure 1. Geometric representation of axisymmetric model with constricting channel with square-edge, 45 degrees angle and fillet edge. The inlet height will vary from 2 mm to 40 mm to account for different diameter ratios.

Cavitation is a function of the localized low pressure which is altered by fluid velocity, turbulence, and principal shear stress. These factors can be affected by fluid properties such as viscosity, geometric properties such as area constriction, and flow properties such as flow rate and inlet turbulence. The diameter ratio was used to represent changes in the geometric area constriction and the mass flow rate was used to represent changes in the flow properties. The results from the simulation were analyzed using non-dimensional numbers to maximize the application of the findings. The computational model proves to be more stable when a mass flow rate is used to control the inlet of the model, rather than a velocity or pressure inlet. For this reason, the density remains constant, so the mass flow rate is the only factor effecting the flow and velocity of the fluid. The density was set to a value equivalent to that of an aqueous solution.

Fluid Model: To generate the CFD model ANSYS Fluent[33] was used. ANSYS Design Modeler and ANSYS Meshing were used to generate the geometric shapes and mesh for each model. Both of these software packages are capable of being run through text commands and are executed through the DOS prompt, allowing the models in each to be manipulated and controlled through a master MATLAB code. The constricting channels were modeled using a 2D axisymmetric algorithm on a HP Z800 Workstation using up to 7 processors. The models ranged in size from 6,000 to 10,000 cells with a maximum cell skewness of 0.36. The model was run in a steady-state format and implemented with a pressure-based implicit volume of fluid solver. A mass transfer between the liquid and gas phases was implemented using the Singhal et. al.[18] full cavitation model. The point at which the fluid underwent a phase change was defined by the liquid critical pressure. This solver utilizes the momentum equation (Equation 9), continuity equation (Equation 10), and the energy equation (Equation 11). A realizable k-ε turbulence model was implemented with standard wall functions. This turbulence model was implemented because it was originally created for modeling internal pipe flows similar to the case exhibited in this fluid model[33]. The turbulence going into the model is considered negligible with respect to the increase in turbulent energy due to the pipe constriction. The fluid properties and flow characteristics were altered for each model and were determined by the master MATLAB code.

Preprints (www.preprints.org) | NOT PEER-REVIEWED | Posted: 7 July 2020 doi:10.20944/preprints202007.0138.v1

$$\frac{\partial}{\partial t}(\rho\vec{v}) + \nabla \cdot (\rho\vec{v}\vec{v}) = -\nabla p + \nabla \cdot (\bar{\bar{\tau}}) + \rho\vec{g} + \vec{F} \quad (9)$$

Where $\vec{v}$ is the velocity vector, ∇ is the derivative in 3 dimensional space, $\bar{\bar{\tau}}$ is the stress tensor, $\vec{g}$ is gravity, and $\vec{F}$ is external body force.

$$\frac{\partial \rho}{\partial t} + \nabla \cdot (\rho\vec{v}) = S_m \quad (10)$$

Where S_m is a mass source term.

$$\frac{\partial}{\partial t}(\rho E) + \nabla\big(\vec{v}(\rho E + p)\big) = \nabla\left(k_{eff}\nabla T - \sum_j h_j\overrightarrow{J_j} + \left(\bar{\bar{\tau}}_{eff} \cdot \vec{v}\right)\right) + S_h \quad (11)$$

Where E is the total fluid energy, k_{eff} is the effective thermal conductivity of the fluid, T is the temperature, h is the enthalpy, J is the diffusion flux, $\bar{\bar{\tau}}_{eff}$ is the effective stress tensor and S_h is a volumetric energy source.

MATLAB Code Setup and Data Generation: An evaluation of the entire design space encompassed by automated pharmaceutical filling machines was utilized to determine the overall risk of cavitation. The fluid properties, flow characteristics, and geometric shape were altered in a systematic manner so each variable could be analyzed independent of the others. Figure 2 is a flow chart outlining the flow of the CFD solver, the mesh generator, and MATLAB codes. The journal files for the meshing and the CFD solvers were altered by MATLAB to encompass the entire design space and the resulting files were run in the command prompt. The Fluent analysis exported text files with the desired outputs from the analysis and MATLAB read the output variables, calculated the desired values, and plotted the results for analysis. The variables perturbed by the MATLAB code are displayed in Table 1. For each of the columns in Table 1, a square-edge, angle, and fillet channels were evaluated producing 280 data points for each channel type. This resulted in 840 data points for the small-scale channel and an additional 840 data points for the large-scale channels. The 1680 different CFD model were then split into cavitating and non-cavitating cases and analyzed.

Preprints (www.preprints.org) | NOT PEER-REVIEWED | Posted: 7 July 2020 doi:10.20944/preprints202007.0138.v1

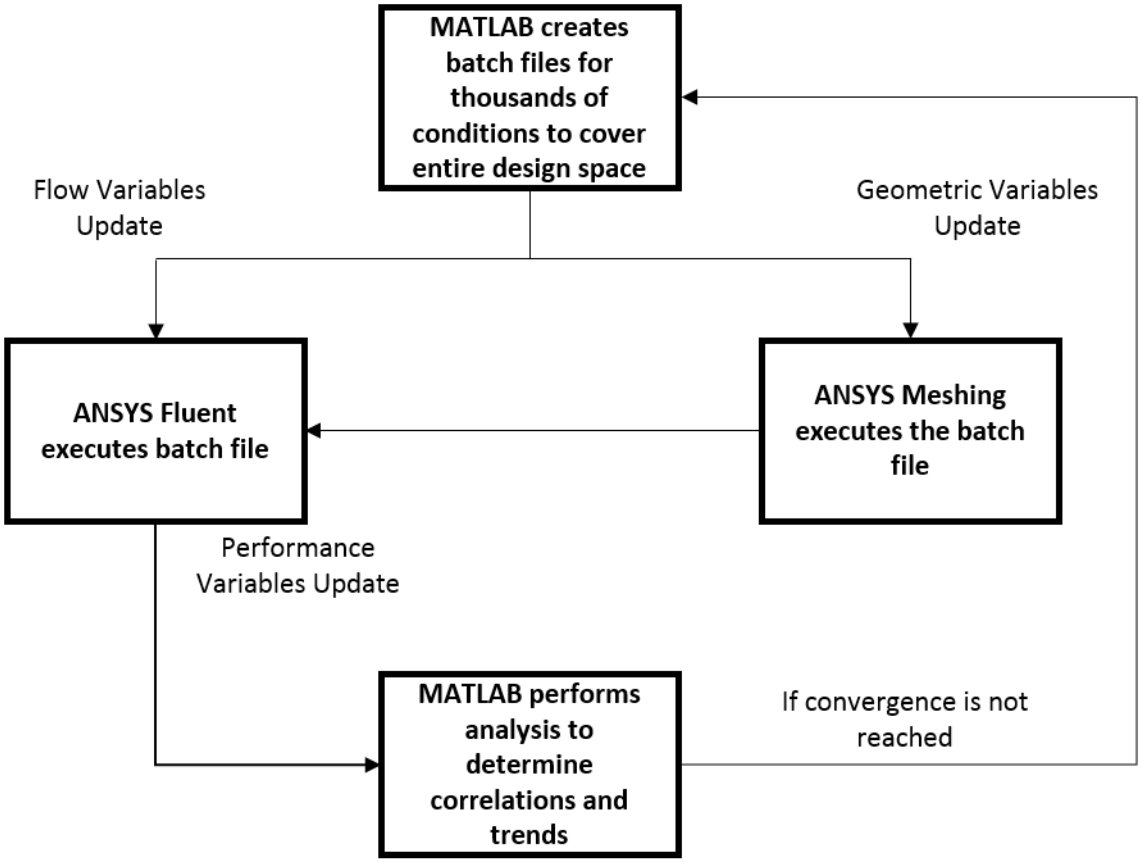

Figure 2. Analysis loop depicting the path by which the software packages pass information to create different models with varying fluid, flow, and geometric properties and then process the results.

Table 1. Conditions at which each of the square-edge, angle, and fillet channels were evaluated resulting in a data point for each model. The operating range, small scale, and large-scale parameters produced 546, 280, and 280 data points respectively for each channel edge type.

	Operating Range	Small Scale	Large Scale
Major Diameter (mm)	5.7, 6.7, 8.0, 10.0, 13.3, 20, 40	8.0, 10.0, 13.3, 20.0	80.0, 100.0, 133.2, 200.0
Minor Diameter (mm)	4	4	4
Flow Rate (kg/s)	0.005, 0.008, 0.010, 0.02, 0.03, 0.04, 0.05, 0.06, 0.08, 0.10, 0.13, 0.16, 0.20	0.01, 0.05, 0.1, 0.12, 0.14, 0.16, 0.18, 0.20, 0.22, 0.24, 0.26, 0.28, 0.30, 0.35	8.0, 9.0, 10.0, 11.0, 12.0, 12.5, 13.0, 13.5, 14.0, 14.5, 15.0, 15.5, 16.0, 17.0
Viscosity (cP)	5.20, 9.34, 16.79, 30.17, 54.2, 97.4	2.89, 5.20, 9.34, 16.79, 30.17	2.89, 5.20, 9.34, 16.79, 30.17
Density (kg/m^3)	1000	1000	1000

Preprints (www.preprints.org) | NOT PEER-REVIEWED | Posted: 7 July 2020 doi:10.20944/preprints202007.0138.v1

Data Analysis Ranges

The range of the variables perturbed by the MATLAB code in Table 1 were chosen to totally encompass the entire design and operating space used by syringe discharge and automated vial and syringe filling. In the manufacturing of theoretic proteins pipe constrictions, needles and syringes can result in diameter ratios from 0.7 to 0.1. This range was chosen because the 0.7 diameter ratio is representative of a minor pipe constriction and 0.1 is representative of a constriction from a syringe to a needle. The mass flow rates were altered from 5 to 200 g/s which represents a slow flow rate used to fill syringes and a fast flow rate used to fill vials[34]. The viscosity of pharmaceutical solutions changes exponentially as a function of solution concentration due to chain entanglement[16]. Therefore, viscosity needs to be represented accurately to provide information on how solution concentration can alter hydrodynamic phenomena. Using the exponential curve generated by Giarratano et. al.[5] the viscosity of the pharmaceutical solution was determined as a function of concentration. The range for protein concentrations ranged from 0 to 20 mg/mL. This resulted in a viscosity range from 2.89 to 30.168 cP. This range essentially represents a range of fluids behavior from water to motor oil. The density was not altered because it was directly related to the mass flow rate. The inlet was modeled as a mass flow inlet, so altering the density would directly alter the flow rate into the system. Therefore, changing the flow rate and density would have the same effect on the system.

Likelihood of Cavitation

To determine if the operating regions of needle expulsion and automated syringe and vial filling are likely to cavitate, the cavitating and non-cavitating data from the likelihood of cavitation column in Table 1 will be analyzed.

Dimensionless Numbers

The data for the square-edge small scale channel was analyzed to determine trends and how to reduce the likelihood of cavitation. To focus on the factors influencing cavitation the minor diameter was held constant and only the square-edge channel was evaluated. This allowed trends to be identified and characterized using non-dimensional and fundamental fluid mechanics numbers.

Edge Constriction Type

To determine if the type of edge has any impact, the mouth of the constriction was altered to a 45 degree angled wall and a smooth fillet wall, Figure 1. The square-edge, 45 degree and fillet channels were each evaluated at the 280 conditions shown in Table 1 column small scale. The results for each channel were compared to determine what effect the edge constriction type has on cavitation.

Geometric Scalability of Diameter

In each of the above models, the minor diameter was held constant and the major diameter was altered to account for the change in diameter ratio. In this section, an additional 280 cases were evaluated for each channel type. The conditions evaluated are shown in Table 1 column large

Preprints (www.preprints.org) | NOT PEER-REVIEWED | Posted: 7 July 2020 doi:10.20944/preprints202007.0138.v1

scale. These data were compared with the previous results of the small scale and together they were used to create threshold bounds for when a fluid flow is likely to cavitate.

Results

Likelihood of Cavitation: The 546 different conditions representing the operating regions of needle expulsion and automated syringe and vial filling resulted in 101 cavitating cases. Figure 3 shows a scatter plot with of diameter ratio versus the Reynolds number with the cavitating and non-cavitating data separated. The model is classified as "cavitation" if any amount of vapor is present. Therefore, there is no measure of intensity of cavitation, just if it is present. The Reynolds number was calculated at the exit of the minor diameter for each case. Overlaid on this data are bounds of operation for various manufacturing and delivery conditions. The operating regions for the syringe discharge, syringe filling, and vial filling operations were determined by the operating conditions of a variety of Bosch pharmaceutical manufacturing products[34]. This figure shows that during needle expulsion, cavitation likely does not occur. However, during syringe and vial filling, cavitation is likely to occur based on the available operating conditions. Both syringe and vial filling run higher risks for cavitation when operating at higher fluid throughputs. This figure clearly demonstrates that cavitation is an issue in pharmaceutical manufacturing and cannot be ignored.

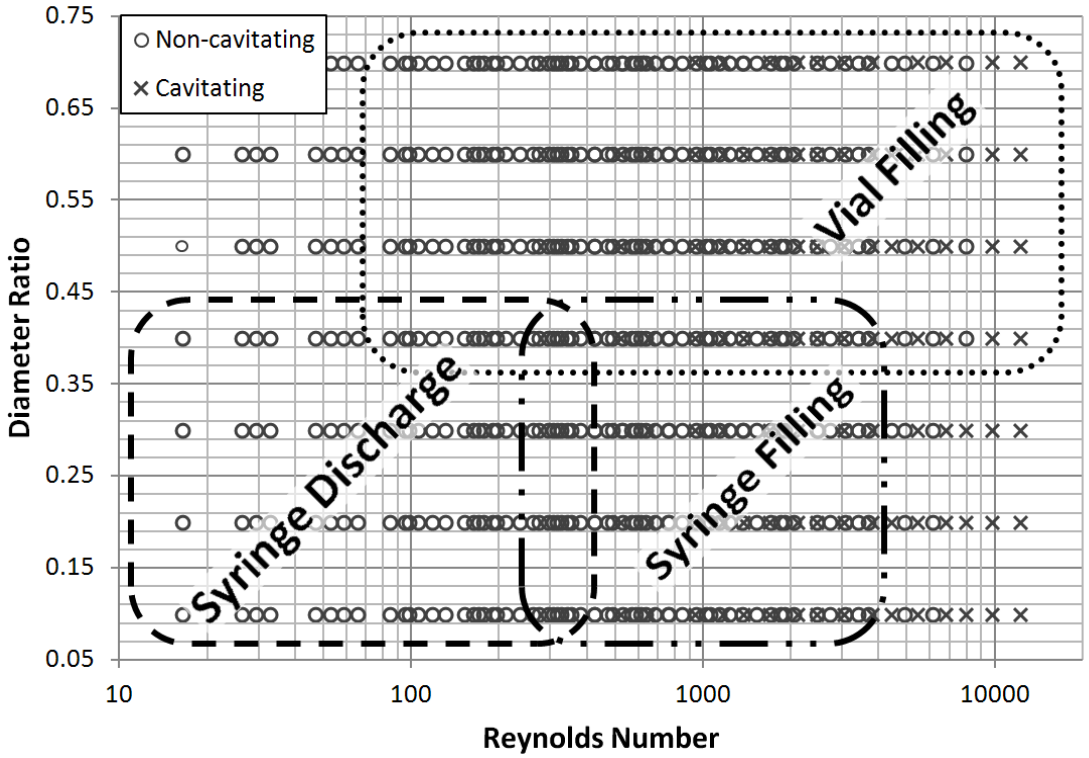

Figure 3. Diameter ratio as a function of the Reynolds Number with the data separated by cavitating and non-cavitating conditions for the square-edge channel. Overlaid on the data are general regions where vial filling, syringe filling, and syringe discharge operations are likely to occur.

Preprints (www.preprints.org) | NOT PEER-REVIEWED | Posted: 7 July 2020 doi:10.20944/preprints202007.0138.v1

Dimensionless Numbers: To analyze the factors associated with the likelihood of cavitation, a better correlation between the fluid flow and fluid properties would need to be better understood. Figure 3 demonstrates that at higher Reynolds number the flow is more likely to cavitate but does not characterize cavitation as a function of the fluid flow and fluid properties. Using different dimensionless and fundamental fluids number, the flow can be analyzed to separate the cavitation and non-cavitating cases. Once separated, trends can be undertaken, and mitigations strategies can be gathered to reduce the likelihood of cavitation. A cavitating flow is a function of the lowest pressure in the fluid region. The low pressure in the fluid is a function of the fluid flow and fluid properties, which could make it a leading candidate for separating the cavitating and non-cavitating groups. Figure 4 shows that if the Reynolds number is below 1000, the fluid will not cavitate, but the figure does not give further insight into what happens if the flow is above a Reynolds number of 1000. It also shows that if the low pressure of the fluid is above 20 KPa the flow will not cavitate, and if it is below it is likely to cavitate with only a few cases where cavitation does not occur. This plot begins to lead to a separation of the cavitating and non-cavitating groups but does not explore the key issue of what is causing cavitation. Therefore, another dimensionless or fundamental fluids number is needed.

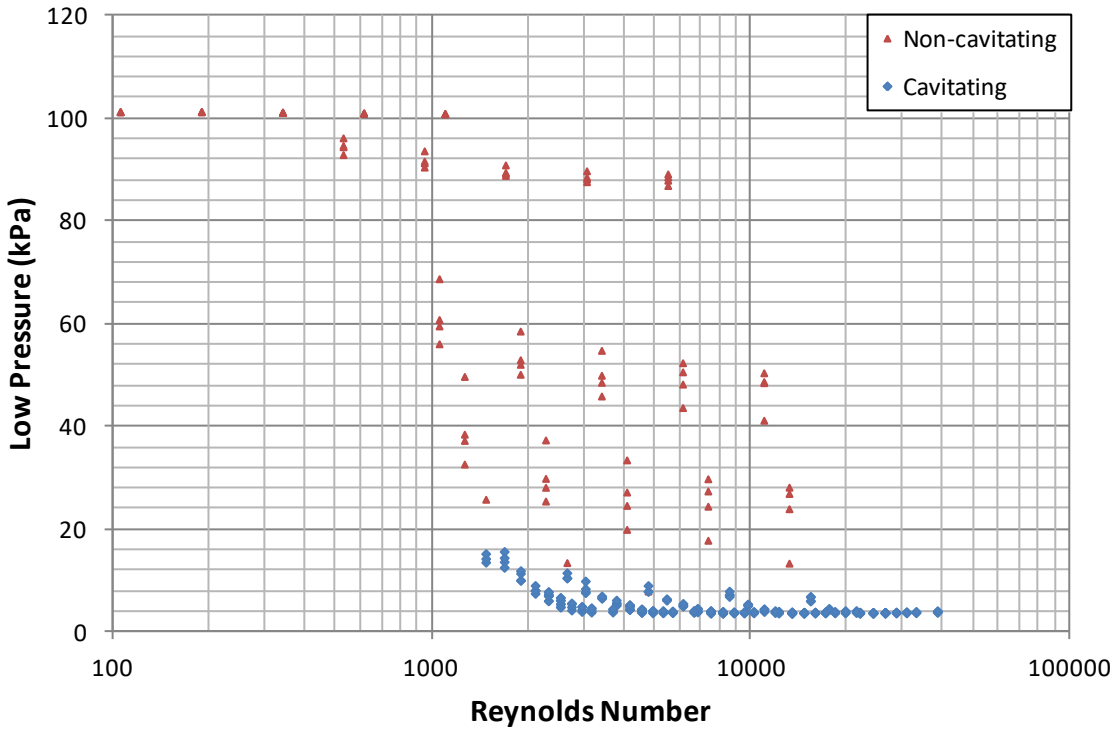

Figure 4. Local low pressure versus the Reynolds number for a constricting, square-edge channel using 546 Fluent models with data separated by cavitating and non-cavitating groups.

The pressure recovery coefficient is a function of the pressure difference and kinetic energy of the fluid which make it a good candidate for separating the cavitating and non-cavitating regions. Figure 5 shows the pressure recovery coefficient versus Reynolds number with the data separated into groups as a function of diameter ratio, w. The data separates nicely with little overlapping regions. However, Figure 6 shows the pressure recovery coefficient as a function of Reynolds

Preprints (www.preprints.org) | NOT PEER-REVIEWED | Posted: 7 July 2020 doi:10.20944/preprints202007.0138.v1

number with the data separated into cavitating and non-cavitating groups, with large areas of overlap. The figures begin to show a separation of cavitating and non-cavitating data, but they were not able to describe a universal threshold bound.

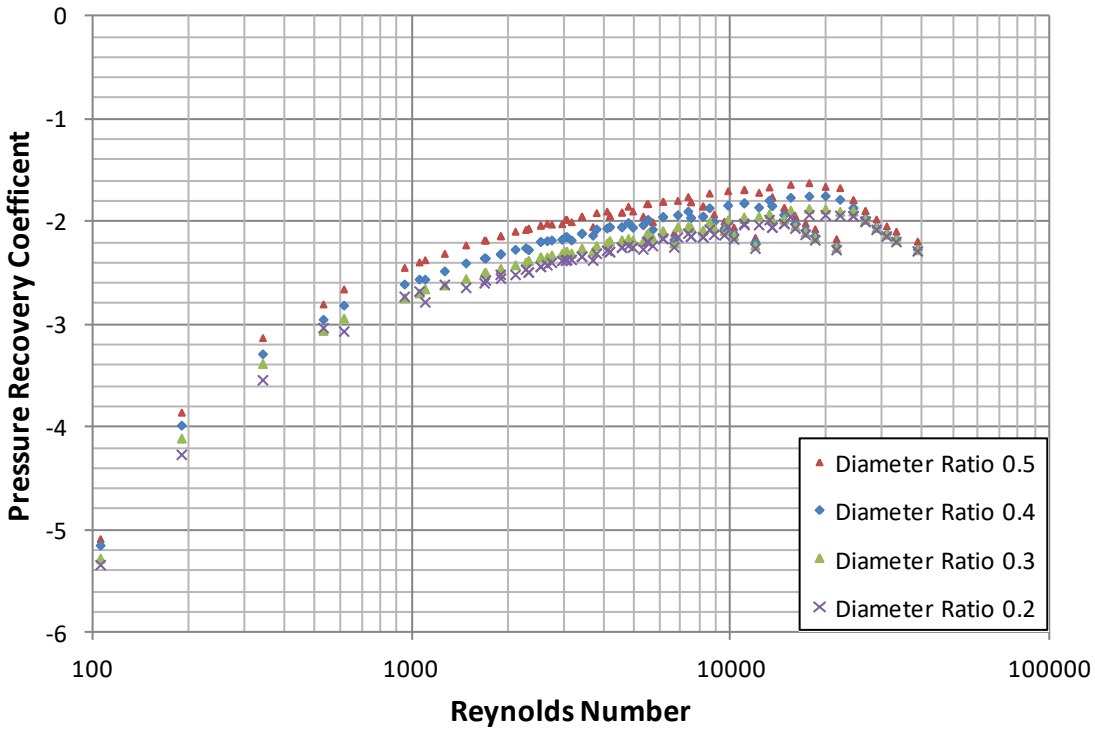

Figure 5. Pressure recovery coefficient versus the Reynolds number for a constricting, square-edge channel using 280 Fluent models with contour of diameter ratio.

Preprints (www.preprints.org) | NOT PEER-REVIEWED | Posted: 7 July 2020 doi:10.20944/preprints202007.0138.v1

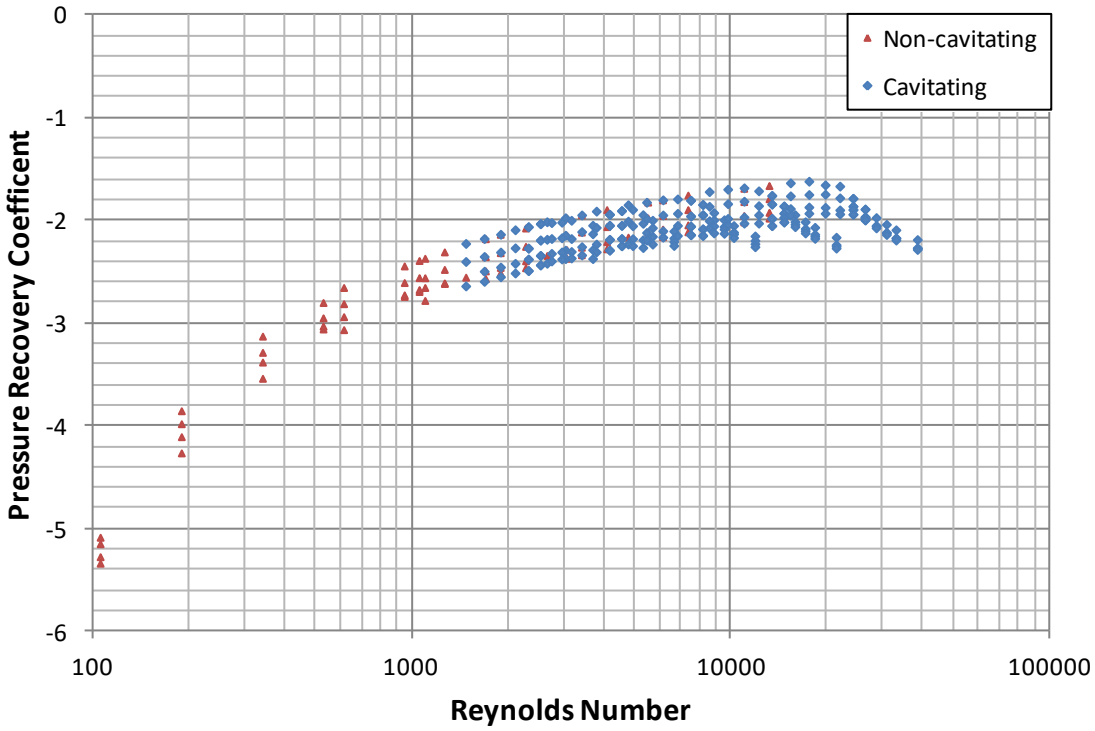

Figure 6. Pressure recovery coefficient versus the Reynolds number for a constricting, square-edge channel using 280 Fluent models with data separated into cavitating and non-cavitating groups.

The Cavitation number is a dimensionless quantity that describes how likely a flow is to cavitate. The Cavitation number is a function of the low pressure in the fluid and the kinetic energy. The velocity term in the Cavitation number is with respect to the outlet velocity in the minor diameter. Figure 7 plots the Cavitation number as a function of the Reynolds number with the data separated into cavitating and non-cavitating groups. This figure shows that if the Cavitation number is below ~0.2, cavitation will likely occur for the type of design and conditions tested in this work. Under the conditions considered here, there are many cases where the fluid does not cavitate under a cavitation number of 1. A threshold of cavitation is sensitive to the materials and parameters being considered[35].

Preprints (www.preprints.org) | NOT PEER-REVIEWED | Posted: 7 July 2020 doi:10.20944/preprints202007.0138.v1

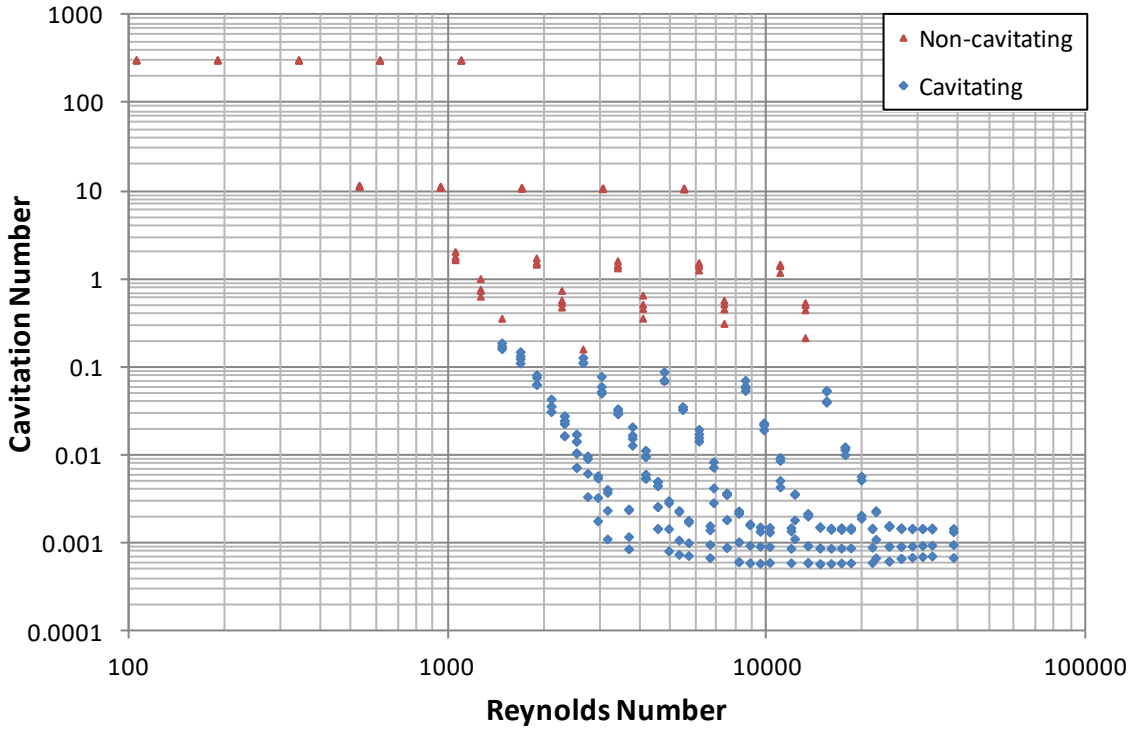

Figure 7. Cavitation number versus the Reynolds number for a constricting, square-edge channel using 280 Fluent models with data separated by cavitating and non-cavitating groups.

The Kolmogorov length scale represents energy dissipation through viscous effects thus providing detailed information on turbulent strength or intensity. Figure 8 shows the Kolmogorov length scale as a function of the Reynolds number with a contour of diameter ratio. A linear relationship between the logarithm of the Kolmogorov length scale and logarithm of the Reynolds number indicates that the Reynolds number and diameter ratio can be captured in the single robust quantity of the Kolmogorov length scale. Figure 9 shows the Kolmogorov length scale as a function of the Reynolds number with cavitating and non-cavitating groups. Again, there are regions of overlapping cavitating and non-cavitating data, but the relationship between Kolmogorov length scale and Reynolds number still hold strong. With the understanding of the relationship between the Kolmogorov length scale and the Reynolds number, it is worthwhile to plot the Cavitation number versus Kolmogorov length scale. Figure 10 shows the Cavitation number versus Kolmogorov length scale with cavitating and non-cavitating groups with a reasonable separation between the cavitating and non-cavitating groups.

Preprints (www.preprints.org) | NOT PEER-REVIEWED | Posted: 7 July 2020 doi:10.20944/preprints202007.0138.v1

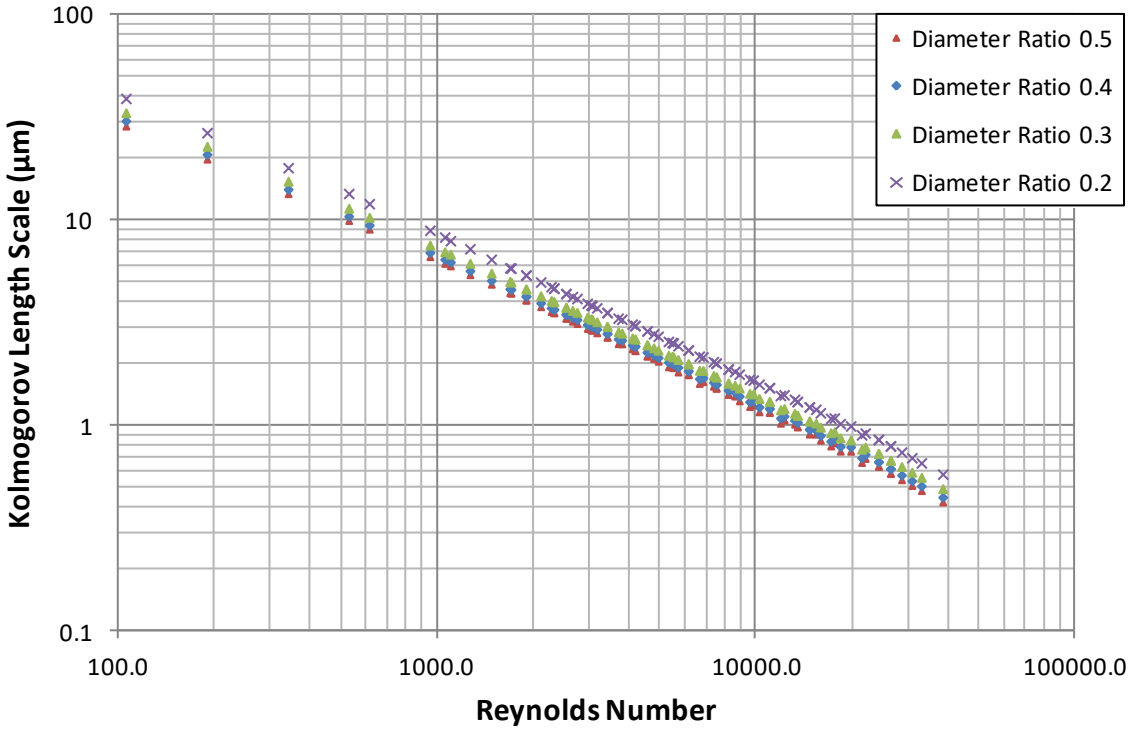

Figure 8. Kolmogorov length scale versus the Reynolds number for constricting square-edge using the 280 Fluent models with the data separated by diameter ratios.

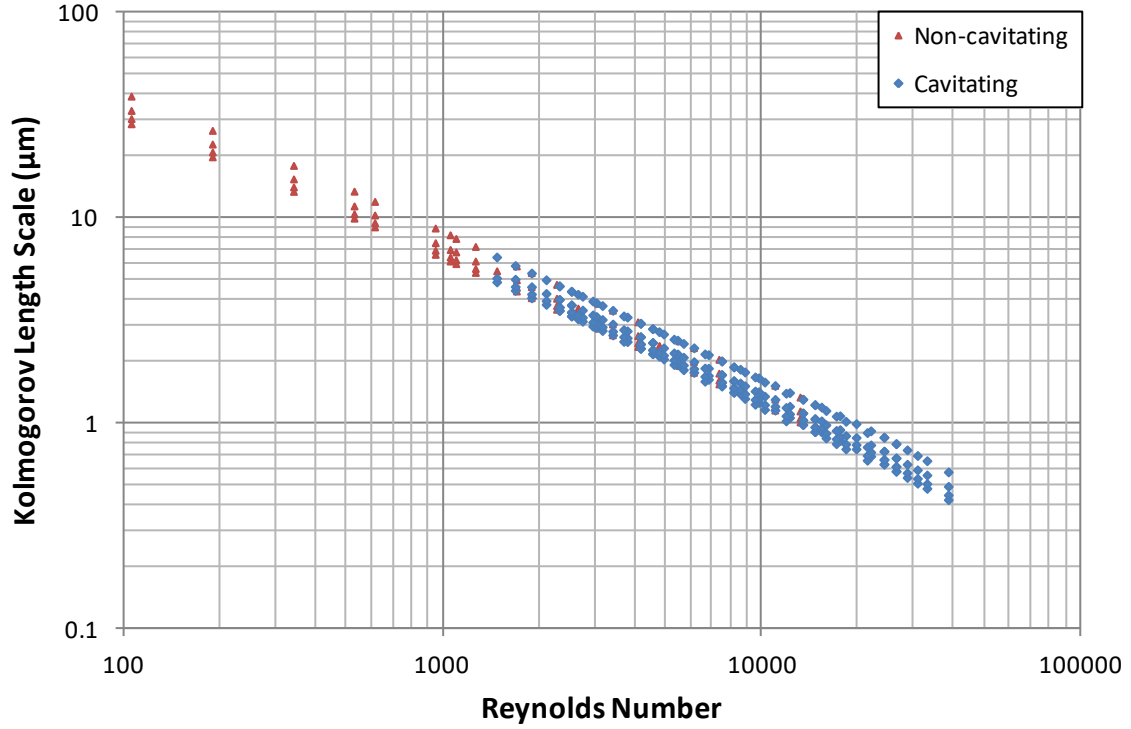

Figure 9. Kolmogorov length scale versus the Reynolds number for constricting square-edge using the 280 Fluent models with the data separated cavitating and non-cavitating groups.

Preprints (www.preprints.org) | NOT PEER-REVIEWED | Posted: 7 July 2020 doi:10.20944/preprints202007.0138.v1

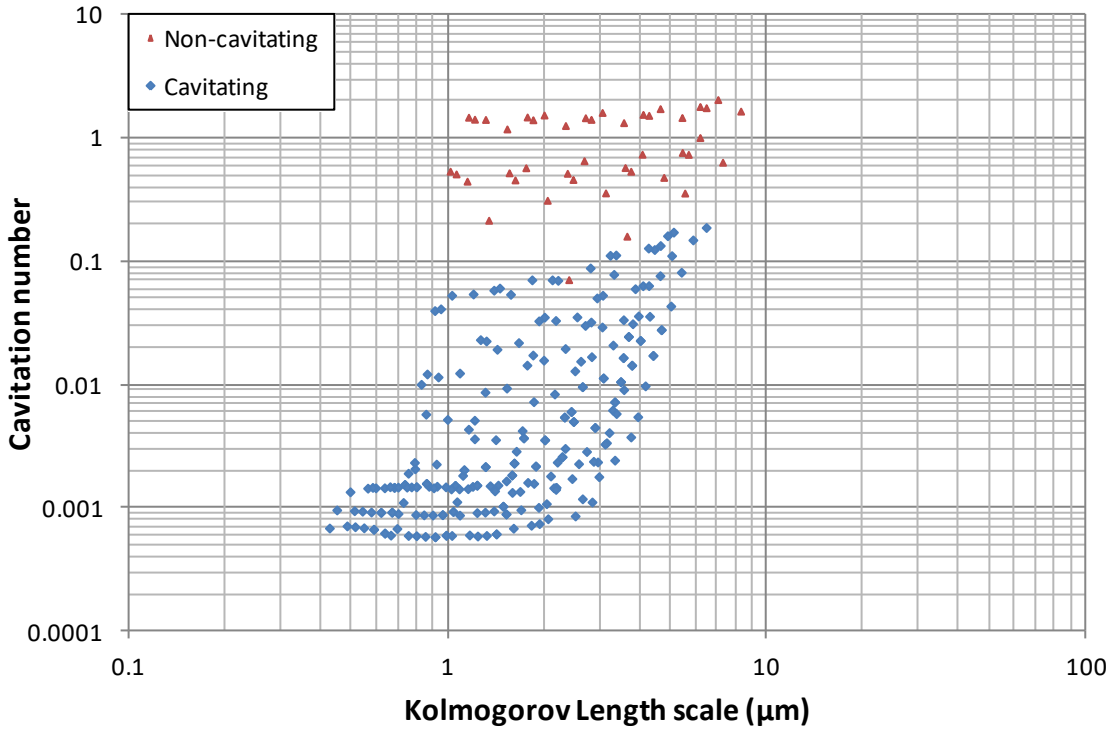

Figure 10. Cavitation number versus Kolmogorov length scale for square-edge constriction channel.

Edge Constriction Types*:* To this point, all of the data analyzed have been for a square-edge constriction channel. By changing the type of edge constriction, a smoother transition from the larger diameter to the smaller diameter can be made. This would change the amount of turbulence introduced at the construction resulting in a change of critical pressure and low pressure. Together this will change the likelihood for a fluid to cavitate. In addition to the square edge channel, the 45 degrees angle and fillet edge channel were analyzed. Due to the nature of the edge types, the square-edge channel has the most turbulent energy and the fillet channel has the least. The same 280 conditions, Table 1 column small scale, were evaluated for the 45 degrees angle and the fillet channels. Figure 11 shows the data from the square-edge, 45 degree, and fillet channels plotted as the Cavitation number versus Reynolds number. If a cavitation, transition, and non-cavitating regions are created, the fluid can be generalized by the following:

Cavitation	if	$C_a < 0.02$
Transition	if	$0.02 < C_a < 0.2$
Non-cavitation	if	$C_a > 0.2$

The most revealing fact about the edge constriction is how much effect it has on the likelihood of the flow to cavitate. The mean critical pressure does not change much, but the low pressure of the fluid in the channel has a large effect. For the same 280 conditions the square-edge, 45 degree, and fillet channels resulted in 237, 194, and 8 cavitating cases, respectively. A comparison of the three channels is seen in Table 2.

Preprints (www.preprints.org) | NOT PEER-REVIEWED | Posted: 7 July 2020 doi:10.20944/preprints202007.0138.v1

Table 2. Results from the square-edge, 45 degree and fillet channels under the 280 conditions outlined in Table 1 column small scale.

	Square-edge	Angle channel	Fillet channel
Atmospheric pressure (kPa)	101.3	101.3	101.3
Vapor pressure (kPa)	3.6	3.6	3.6
Mean critical pressure (kPa)	5.9	10.4	10
Mean low pressure (kPa)	21	34.5	85.8
Cavitating models	237	194	8
Non-Cavitating models	43	86	272
Total Models	280	280	280

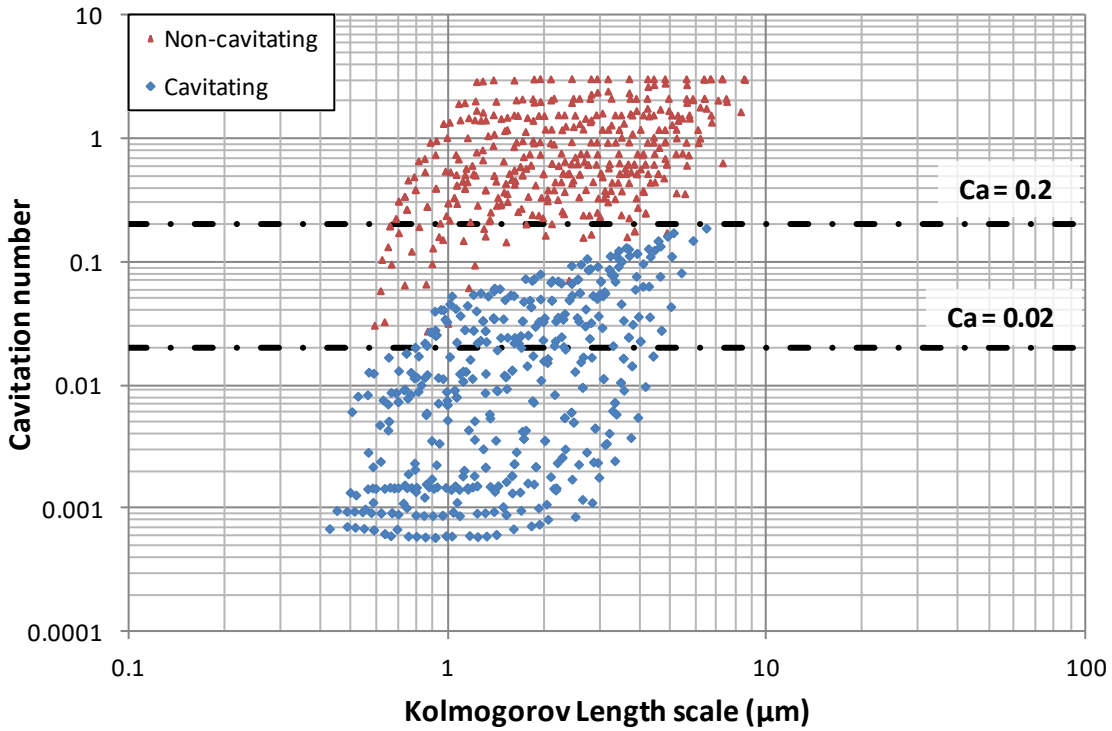

Figure 11. Cavitation number versus Kolmogorov length scale for square-edge, 45 degree, and fillet channels separated into cavitating and non-cavitating groups. Threshold bounds are applied to show a cavitating, transition, and non-cavitating regions.

Geometric Scalability of Diameter: For each of the previous models the minor diameter was held constant and the major diameter was altered to accommodate the change in diameter ratio. It is of interest to know if these threshold bounds can be translated to constricting channels of different scales. A constricting square-edge, 45 degree, and fillet channels were analyzed under the conditions of Table 1 column large scale. Figure 12 shows the Cavitation number versus Kolmogorov length scale for the three edge constriction types with data grouped into cavitating and non-cavitating cases. Additionally, the same threshold bounds created from the previous section are applied. Under these conditions the large-scale data fall into the same bounds as the

Preprints (www.preprints.org) | NOT PEER-REVIEWED | Posted: 7 July 2020 doi:10.20944/preprints202007.0138.v1

small-scale data. Figure 13 shows the large scale and small-scale data with all three channel types fitting into the same threshold bounds. These data show the first quantifiable threshold bound for a cavitating flow with respect to the Cavitation number.

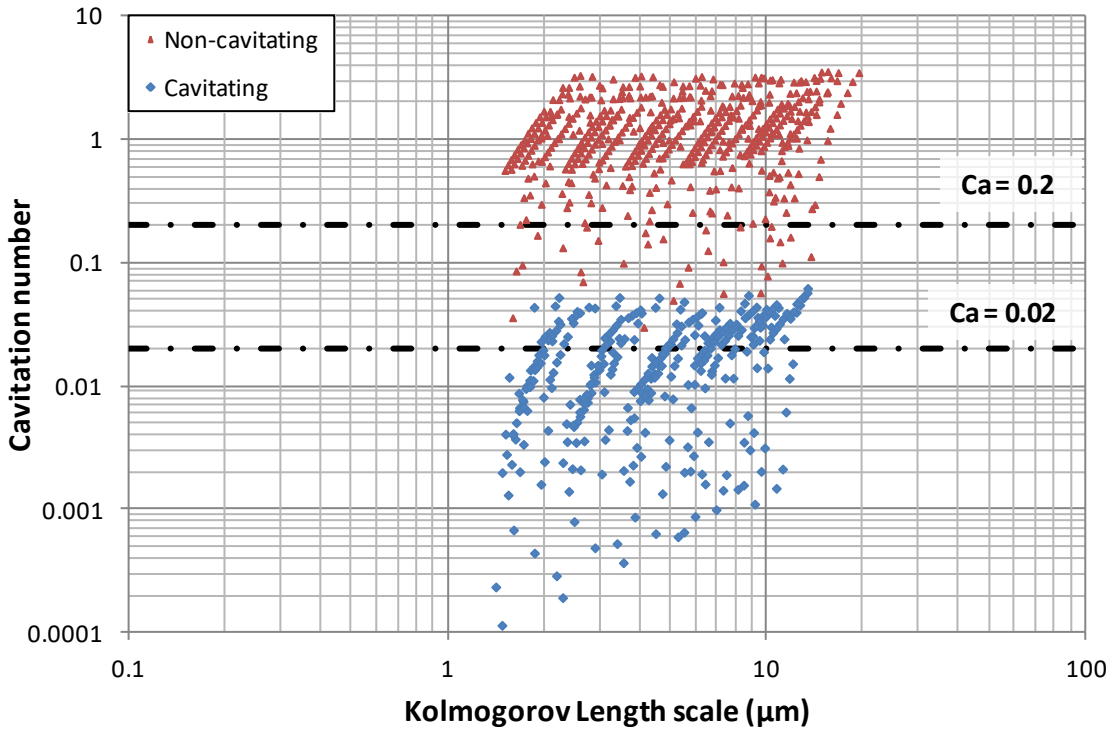

Figure 12. Cavitation number versus Kolmogorov length scale for the large square-edge, 45 degree, and fillet channels separated into cavitating and non-cavitating groups. The same threshold bounds are applied as with the small scale and resulting the large-scale data fitting into the same cavitating, transition, and non-cavitating regions.

Preprints (www.preprints.org) | NOT PEER-REVIEWED | Posted: 7 July 2020 doi:10.20944/preprints202007.0138.v1

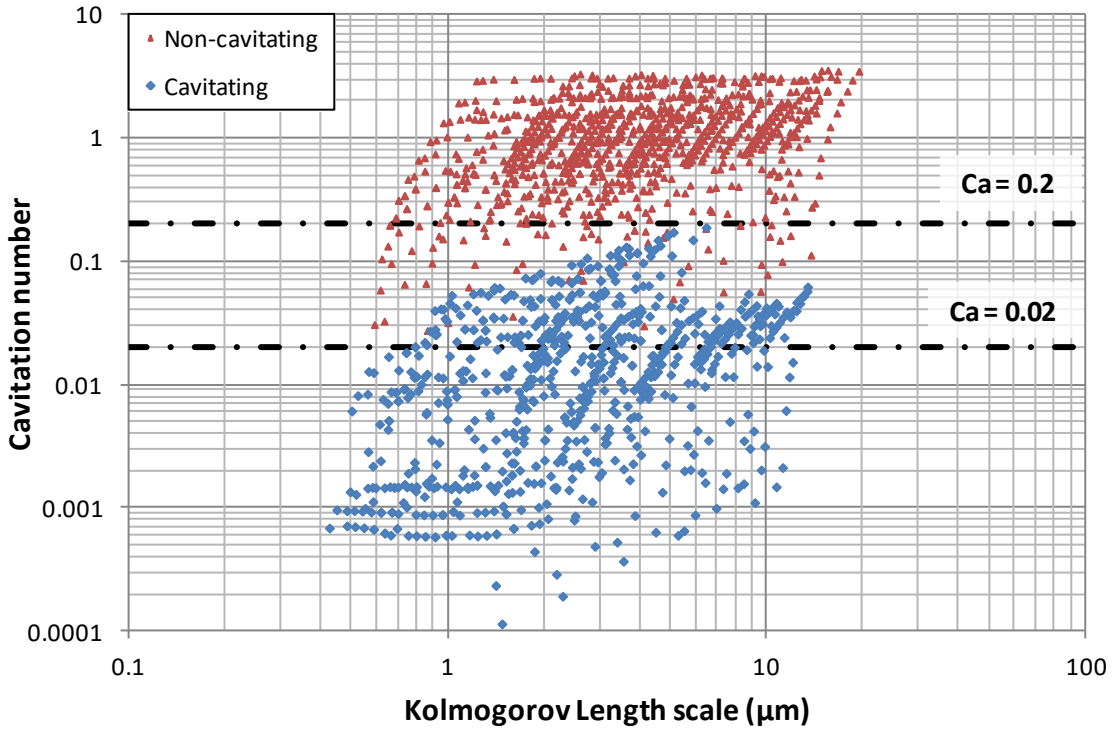

Figure 13. Cavitation number versus Kolmogorov Length scale for the large and small- scale diameter channels. Overlaid on top of the combined data are bounds describing the cavitating, transition, and non-cavitating regions.

Discussion and Recommendations for Pharmaceutical Industry: The application of these findings with respect to pharmaceutical manufacturing demonstrates that cavitation is a problem in vial and syringe filling. However, when developing new manufacturing systems, steps can be taken to reduce the likelihood of cavitation. The largest and perhaps easiest impact would be to add a fillet to every edge, but this is not always feasible, so at minimum a tapered edge should be utilized. This smoothing of the edge type should be applied in piping systems, pumps, and valves. Next, much more thought should be applied to reducing the amount of turbulence introduced into the system. Finally, the Cavitation number should be calculated and applied to the threshold boundary conditions to determine if the flow is in a cavitating, transition, or non-cavitating region. If these steps are taken when designing new pharmaceutical manufacturing systems, the likelihood of cavitation can be greatly reduced. Proof of this is evident when comparing the number of cavitating cases in the square-edge channels to that in the fluid channels, 237 compared to 8, respectively. Prefilled syringes may experience protein stability problems. Previous studies evaluated the influence of several parameters on protein stability including the effects of surfactants to reduce protein surface adsorption in syringes[10,36,37], syringe and tip cap material[38,39], storage[38,40,41], the use of silicone oil-free technologies[42,43], agitation[10,38,41], temperature[41], and manufacturing technology[44]. The literature concerning the links between the occurrence of cavitation according to syringe geometrical parameters (i.e. pipe contraction) is still missing in the pharmaceutical industry. This gap in the literature motivated this research. Particularly, this

computational work approached the influence of geometrical parameters on the onset of cavitation in syringes, consequently leading to subvisible particle formation and protein aggregation.

Conclusions

This research shows under current pharmaceutical manufacturing conditions, especially in automated vial and syringe filling operations, cavitation is a real risk that needs to be quantified and mitigated. The most universal method in determining the risk of cavitation is by calculating the Cavitation number and determining which region the flow is operating in. Considering the conditions found in syringe injection and rapid vial filling that were simulated in the present study, if the Cavitation number is larger than 0.2, the fluid will not cavitate. For different conditions not being considered here, it is recommended that modeling of cavitation inception be performed following the guidelines provided in this present study. To increase the cavitation number one can remove sharp edges by rounding, or reduce turbulence by reducing the mass flow rate or increasing the viscosity. These conditions most likely occur at the outlet of pumps, valves, and reductions in cross sectional area (i.e. fill needles).

References

1. Chi, E. Y.; Krishnan, S.; Randolph, T. W.; Carpenter, J. F. Physical Stability of Proteins in Aqueous Solution: Mechanism and Driving Forces in Nonnative Protein Aggregation. *Pharm Res*, **20** (9), 1325–36. https://doi.org/10.1023/A:1025771421906 (2003).

2. Manning, M.C.; Chou; D.K.; Murphy; B.M.; Payne, R.W.; Katayama, D.S. Stability of Protein Pharmaceuticals: An Update. *Pharm Res*, **27** (4), 544–75. https://doi.org/10.1007/s11095-009-0045-6 (2010).

3. Stefani, M.; Dobson, C.M. Protein aggregation and aggregate toxicity: new insights into protein folding, misfolding diseases and biological evolution. *J Molec Medic*, **81**(11), 678–99, https://doi.org/10.1007/s00109-003-0464-5 (2003).

4. Fink, A.L. Protein aggregation: folding aggregates, inclusion bodies and amyloid. *Folding & design*, **3** (1), R9–R23. https://doi.org/10.1016/S1359-0278(98)00002-9 (1998).

5. Giarratano, J. Protein Aggregation Through Acoustic Cavitation. Msc Thesis, University of Denver, 2012.

6. Randolph, T. W.; Schiltz, E.; Sederstrom, D.; Steinmann, D.; Mozziconacci, O.; Schöneich, C.; Freund, E.; Ricci, M. S.; Carpenter, J. F.; Lengsfeld, C. S. Do not drop: mechanical shock in vials causes cavitation, protein aggregation, and particle formation. *J Pharm Sci*, **104** (2), 602-611, https://doi.org/10.1002/jps.24259 (2015).

7. Torisu, T.; Maruno, T.; Hamaji, Y.; Ohkubo, T.; Uchiyama, S. Synergistic Effect of Cavitation and Agitation on Protein Aggregation. *J Pharm Sci*, **106**, 521-529, https://doi.org/10.1016/j.xphs.2016.10.015 (2017).

8. Nejadnik, M. R.; Randolph, T. W.; Volkin, D. B.; Schöneich, C.; Carpenter, J. F.; Crommelin, D. J.; Jiskoot, W. Postproduction handling and administration of protein pharmaceuticals and

potential instability issues. *J Pharm Sci.*, **107**(8), 2013-2019, https://doi.org/10.1016/j.xphs.2018.04.005 (2018).

9. Rosenberg, A.; Sauna, Z. Immunogenicity assessment during the development of protein therapeutics. *J Pharm Pharmacol*, **70**(5), 584-594, https://doi.org/10.1111/jphp.12810 (2018).
10. Gerhardt, A.; Mcgraw, N. R.; Schwartz, D. K.; Bee, J. S.; Carpenter, J. F.; Randolph, T. W. Protein aggregation and particle formation in prefilled glass syringes. *J Pharm Sci*, ***103*** (6): 1601-1612, https://doi.org/10.1002/jps.23973 (2014).
11. Cromwell, M.E.M.; Hilario, E.; Jacobson ,F. Protein Aggregation and Bioprocessing. *The AAPS journal*, **8** (3), E572–E579. https://doi.org/10.1208/aapsj080366 (2006).
12. DiMasi, J.A.; Hansen, R.W.; Grabowski, H. G. The price of innovation: new estimates of drug development costs. *J Health Econ*, **22** (2), 151–85, https://doi.org/10.1016/s0167-6296(02)00126-1 (2003).
13. Sivakumar, M.; Tang, S.Y.; Tan, K.W. Cavitation technology - A greener processing technique for the generation of pharmaceutical nanoemulsions. *Ultrason Sonochem*, **21**, 2069–2083. https://doi.org/10.1016/j.ultsonch.2014.03.025 (2014).
14. Hong, D.X.; Yun, Y.L.; Guan, Y.X.; Yao, S.J. Preparation of micrometric powders of parathyroid hormone (PTH1–34)-loaded chitosan oligosaccharide by supercritical fluid assisted atomization. *Int J Pharm*, **545**, 389–394. https://doi.org/10.1016/j.ijpharm.2018.05.022 (2018).
15. Ciriminna R.; Albanese, L.; Meneguzzo, F.; Pagliaro, M. Wastewater remediation via controlled hydrocavitation. *Environ Rev*, **25**, 175–183. https://doi.org/10.1139/er-2016-0064 (2017).
16. Poling, B. E.; Prausnitz, J. M.; O'Connell; J.P. *The Properties of Gases and Liquids*, 5th ed., McGraw-Hill: New York, United States of America, pp. 7.3–7.7 (2000).
17. Cui, J.; Lai, H.; Feng, K.; Ma, Y. Quantitative analysis of the minor deviations in nozzle internal geometry effect on the cavitating flow. *Exp Therm Fluid Sci*, **94**, 89–98. https://doi.org/10.1016/j.expthermflusci.2018.02.002 (2018).
18. Singhal, A.K.; Athavale; M.M.; Li, H.; Jiang, Y. Mathematical Basis and Validation of the Full Cavitation. *J Fluids Eng*, **124**, 617–624. https://doi.org/10.1115/1.1486223 (2002).
19. Kumar, P.S.; Pandit, A.B. Modeling hydrodynamic cavitation. *Chem Eng Technol*, **22**, 1017–1027. https://doi.org/10.1002/(SICI)1521-4125(199912)22:12<1017::AID-CEAT1017>3.0.CO;2-L (1999).
20. Kubota A.; Kato, H.; Yamaguchi, H. A new modelling of cavitating flows: a numerical study of unsteady cavitation on a hydrofoil section. *J Fluids Eng*, **240**, 59–96. https://doi.org/10.1017/s002211209200003x (1992).
21. Wang, Y.; Brennen, C. E. Shock wave development in the collapse of a cloud of bubbles. *ASME*, 194, 15–19. (1994).

22. Keller, A.; Rott, H. The Effect of Flow Turbulence on Cavitation Inception. *In Proceedings ASME Fluids Engineering Division Meeting*, 1-8. (1997)

23. Hsiao, C.; Pauley, L. Numerical Study of Tip Vortex Cavitation Inception Using a Bubble Dynamics Model," *In Proceedings ASME Fluids Engineering Division Meeting, 1997.*

24. Choi, J.K.; Kinnas; S.A. Cavitating Propeller Analysis of a Tunnel. *In Proceedings ASME Fluids Engineering Division Meeting*, 1997.

25. Patella, R.F.; Reboud, J.L. A New Approach to Evaluate the Cavitation Erosion Power. *J Fluids Eng*, **120** (2), 335–344. https://doi.org/10.1115/1.2820653 (1998).

26. Kunz; R. F.; Chyczewski, T. S.; Stinebring; D. R.; Gibeling; H. J. Multi-phase cfd analysis of natural and ventilated cavitation about submerged bodies. ASME Fluids Engineering Conference, 2–9, San Francisco (California), United States of America (1999).

27. Avva, R.; Singhal, A.; Gibson, D. An Enthalpy Based Model of Cavitation. *ASME Paper*, vol. 226, pp. 63–70, (1995).

28. Randolph, T.; Schiltz, E. Effect of mechanical shock on protein aggregation and particle formation. in Workshop on Protien Aggregation and Immungicity 2, Breckenridge (Colorado), United States of America (2012).

29. Wu, H. Studies on the Denaturation of proteins, XIII. A theory of denaturation. *Adv Protein Chem*, **46**, 6-26. https://doi.org/10.1016/s0065-3233(08)60330-7 (1995).

30. Rodrigues, R.V.; Puryear, M.; Sederstrom, D.; Lengsfeld, C.S. Parameters influencing cavitation within vials subjected to drop shock. *Sci Rep*, **9**, 19210. https://doi.org/10.1038/s41598-019-55668-9 (2019).

31. Martínez-Monteagudo, S.I.; Yan, B.; Balasubramaniam, V.M. Engineering process characterization of high-pressure homogenization—from laboratory to industrial scale. *Food Eng Rev*, **9**, 143–169, https://doi.org/10.1007/s12393-016-9151-5. (2017).

32. Lengsfeld, C. S.; Munson, L.; Lentz, Y. K.; Anchordoquy, T.J. DNA Hydrodynamic Degradation Controlled by Kolomogorov Length Scales in Pipe Flow. *J Pharm Sci*, **100** (8), 3088–3095. https://doi.org/10.1002/jps.22582 (2011).

33. ANSYS, "Fluent Users." [Online]. Available: www.Fluentusers.com.

34. Bosch_LLC, "Bosch Products," 2012. [Online]. Available: http://www.boschpackaging.com/Boschpharma-us/eng/64350_63978.asp#.

35. Šarc, A.; Stepišnik-Perdih, T.; Petkovšek, M.; Dular, M. The issue of cavitation number value in studies of water treatment by hydrodynamic cavitation. *Ultrason Sonochem* 34, 51–59. https://doi.org/10.1016/j.ultsonch.2016.05.020 (2017).

36. Felsovalyi, F.; Janvier, S.; Jouffray, S.; Soukiassian, H.; Mangiagalli, P. Silicone-oil-based subvisible particles: Their detection, interactions, and regulation in prefilled container closure systems for biopharmaceuticals. *J Pharm Sci*, ***101*** (12), 4569-4583. https://doi.org/10.1002/jps.23328 (2012).

37. Rudiuk, S; Cohen-Tannoudji, L. ; Huille, S.; Tribet, C. Importance of the dynamics of adsorption and of a transient interfacial stress on the formation of aggregates of IgG antibodies. *Soft Matter*, **8** (9), 2651-2661. https://doi.org/10.1039/c2sm07017k (2012).

38. Badkar, A.; Wolf, A.; Bohack, L.; Kolhe, P. Development of biotechnology products in pre-filled syringes: technical considerations and approaches. *Aaps Pharmscitech*, **12** (2), 564-572. https://doi.org/10.1208/s12249-011-9617-y (2011).

39. Krayukhina, E.; Tsumoto, K.; Uchiyama, S.; Fukui, K. Effects of syringe material and silicone oil lubrication on the stability of pharmaceutical proteins. *J Pharm Sci*, **104** (2), 527-535. https://doi.org/10.1002/jps.24184 (2015).

40. Khalili, H.; Sharma, G.; Froome, A.; Khaw, P.T.; Brocchini, S. Storage stability of bevacizumab in polycarbonate and polypropylene syringes. *Eye*, **29** (6), 820-827. https://doi.org/10.1038/eye.2015.28 (2015).

41. Majumdar, S.; Ford, B.M.; Mar, K.D.; Sullivan, V.J.; Ulrich, R.G.; D'souza, A.J.M. Evaluation of the effect of syringe surfaces on protein formulations. *J Pharm Sci*, **100** (7), 2563-2573. https://doi.org/10.1002/jps.22515 (2011).

42. Yoshino, K.; Nakamura, K.; Yamashita, A.; Abe, Y.; Iwasaki, K.; Kanazawa, Y.; Funatsu,K.; Yoshimoto, T.; Suzuki, S. Functional evaluation and characterization of a newly developed silicone oil-free prefillable syringe system. *J Pharm Sci*, **103** (5), 1520-1528. https://doi.org/10.1002/jps.23945 (2014).

43. Depaz, R. A.; Chevolleau, T.; Jouffray, S.; Narwal, R.; Dimitrova, M. N. Cross-linked silicone coating: a novel prefilled syringe technology that reduces subvisible particles and maintains compatibility with biologics. *J Pharm Sci*, **103** (5), 1384-1393. https://doi.org/10.1002/jps.23947 (2014).

44. Rodrigues R.V., Lengsfeld C.S., "Rotary Piston Pump CFD Model to Explore Sub Visible Particle Formation," Workshop on Protein Aggregation and Immunogenicity 2018, Breckenridge (Colorado), United States of America (2018).

Authors Contribution

D.S. designed the simulations, performed the simulations, analyzed the dataset, manuscript writing, reviewing and formatting. R.V.R. performed the simulations, helped to analyze the dataset, manuscript writing, reviewing and formatting. C.L. supervised the project, designed the simulations, performed the simulations, helped to analyze the dataset, manuscript reviewing.